NASA/CR—2003-212714

Pulsed Inductive Thruster (PIT): Modeling and Validation Using the MACH2 Code

Pavlos G. Mikellides
Arizona State University, Tempe, Arizona

December 2003

The NASA STI Program Office . . . in Profile

Since its founding, NASA has been dedicated to the advancement of aeronautics and space science. The NASA Scientific and Technical Information (STI) Program Office plays a key part in helping NASA maintain this important role.

The NASA STI Program Office is operated by Langley Research Center, the Lead Center for NASA's scientific and technical information. The NASA STI Program Office provides access to the NASA STI Database, the largest collection of aeronautical and space science STI in the world. The Program Office is also NASA's institutional mechanism for disseminating the results of its research and development activities. These results are published by NASA in the NASA STI Report Series, which includes the following report types:

- TECHNICAL PUBLICATION. Reports of completed research or a major significant phase of research that present the results of NASA programs and include extensive data or theoretical analysis. Includes compilations of significant scientific and technical data and information deemed to be of continuing reference value. NASA's counterpart of peer-reviewed formal professional papers but has less stringent limitations on manuscript length and extent of graphic presentations.

- TECHNICAL MEMORANDUM. Scientific and technical findings that are preliminary or of specialized interest, e.g., quick release reports, working papers, and bibliographies that contain minimal annotation. Does not contain extensive analysis.

- CONTRACTOR REPORT. Scientific and technical findings by NASA-sponsored contractors and grantees.

- CONFERENCE PUBLICATION. Collected papers from scientific and technical conferences, symposia, seminars, or other meetings sponsored or cosponsored by NASA.

- SPECIAL PUBLICATION. Scientific, technical, or historical information from NASA programs, projects, and missions, often concerned with subjects having substantial public interest.

- TECHNICAL TRANSLATION. English-language translations of foreign scientific and technical material pertinent to NASA's mission.

Specialized services that complement the STI Program Office's diverse offerings include creating custom thesauri, building customized databases, organizing and publishing research results . . . even providing videos.

For more information about the NASA STI Program Office, see the following:

- Access the NASA STI Program Home Page at ***http://www.sti.nasa.gov***

- E-mail your question via the Internet to help@sti.nasa.gov

- Fax your question to the NASA Access Help Desk at 301–621–0134

- Telephone the NASA Access Help Desk at 301–621–0390

- Write to:
  NASA Access Help Desk
  NASA Center for AeroSpace Information
  7121 Standard Drive
  Hanover, MD 21076

NASA/CR—2003-212714

Pulsed Inductive Thruster (PIT): Modeling and Validation Using the MACH2 Code

Pavlos G. Mikellides
Arizona State University, Tempe, Arizona

Prepared for the
28th International Electric Propulsion Conference
cosponsored by the Centre National d'Études Spatiales (CNES), European Office of Aerospace Research and Development of the USAF, Snecma Moteurs, and European Space Agency (ESA)
Toulouse, France, March 17–21, 2003

Prepared under Cooperative Agreement NCC3–860

National Aeronautics and
Space Administration

Glenn Research Center

December 2003

Acknowledgments

The author acknowledges the valuable insights and contributions by R. Lovberg, D. Kirtley, and M. LaPointe. The effort was supported by NASA Glenn Research Center through Ohio Aerospace Institute, SA02–1422.

Available from

NASA Center for Aerospace Information
7121 Standard Drive
Hanover, MD 21076

National Technical Information Service
5285 Port Royal Road
Springfield, VA 22100

Available electronically at http://gltrs.grc.nasa.gov

PULSED INDUCTIVE THRUSTER (PIT): MODELING AND VALIDATION USING THE MACH2 CODE

Pavlos G. Mikellides
Arizona State University
Department of Mechanical and Aerospace Engineering
Tempe, AZ 85287-6106
Phone: 480–727–6215
E-mail: Pavlos.Mikellides@asu.edu

ABSTRACT

Numerical modeling of the Pulsed Inductive Thruster exercising the magnetohydrodynamics code, MACH2 aims to provide bilateral validation of the thruster's measured performance and the code's capability of capturing the pertinent physical processes. Computed impulse values for helium and argon propellants demonstrate excellent correlation to the experimental data for a range of energy levels and propellant-mass values. The effects of the vacuum tank wall and mass-injection scheme were investigated to show trivial changes in the overall performance. An idealized model for these energy levels and propellants deduces that the energy expended to the internal energy modes and plasma dissipation processes is independent of the propellant type, mass and energy level.

INTRODUCTION

The Pulsed Inductive Thruster (PIT) is a unique propulsion system due to a combination of its distinctive physical operation, demonstrated performance and potential advantages over all other electric rockets.[1] A spiral induction coil is powered by a series of capacitors in Marx-loop configurations and produces a strong azimuthal electric field once the pulsed current is passed through. The field breaks down the injected propellant over the surface of the flat coil and the associated radial magnetic field induces an azimuthal current within a thin gas layer (figure 1). This current interacts with the magnetic field to produce an axially-directed electromagnetic force. Such inductive acceleration circumvents the need for electrodes and the erosion-related lifetime limitations that plague traditional electromagnetic thrusters. The PIT can operate with any propellant, however single-shot operation demonstrated optimum performance with polyatomic-molecule fuel. Specifically, the PIT-MkV operating with ammonia at 4.6kJ demonstrated nearly-constant efficiencies exceeding 50% for a wide range of specific-impulse values; 4000s<Isp<8000s. Its propensity to work best with such fuels renders the thruster ideal for water-propellant operation and associated missions such as In-Situ Propellant Utilization (ISRU) where refueling can be realized by appropriate water-rich cometary rendezvous or by capitalizing on Europa's oceans for deeper space assignments. Its pulsed operation can provide elevated maneuverability -- the aforementioned operation produced an impulse range of 0.05N-s<I-bit<0.12 N-s - which in conjunction to its water-propellant affinity establishes the concept very attractive for Orbital Express Architectures during which satellites can refuel and upgrade electronics by docking to on-orbit modules.

In order to provide added confidence in the PIT's demonstrated capabilities the magnetohydrodynamics (MHD) code, MACH2 is employed to model its operation and offer preliminary validation by comparisons with experiments. Specifically, the paper aims to validate the code's capabilities in capturing the pertinent physics by comparing experimental results to the numerical findings.

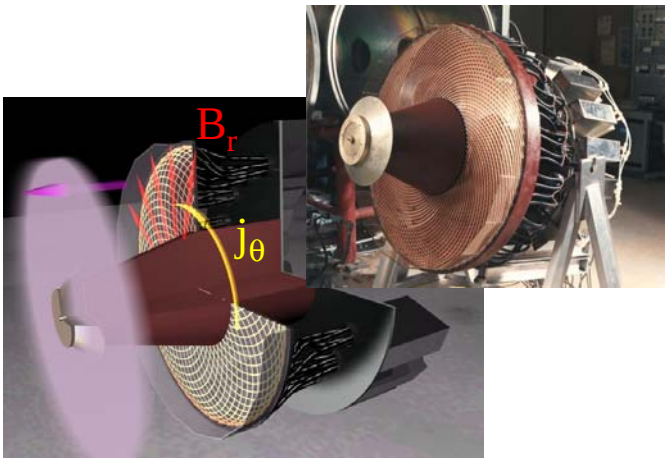

Figure 1.—The Pulsed Inductive Thruster (PIT) (Courtesy TRW) and a schematic of the relative acceleration process due to the dominant interaction of the applied radial field and the induced azimuthal current.

NUMERICAL MODEL

MACH2 is a time-dependent, two-dimensional, axisymmetric, multi-material code that can be applied to problems of complex geometries due to its multi-block structure.[2] The computational mesh can move in an Arbitrary-Lagrangian-Eulerian (ALE) fashion allowing applicability to both diffusive-and dispersive-dominated problems as well as code validation. The mesh can be refined via a variety of adaptive schemes to capture regions of varying characteristic scale. The set of the single-fluid, MHD equations is time-advanced with finite-volume spatial differencing, and the boundary conditions are applied via the ghost-cell technique so that no special conditional statement is necessary at the boundaries.

The mass continuity and momentum equations assume a compressible, viscous fluid with the latter including both real and artificial viscosity effects. The stress-deviator can be chosen to evolve under elastic stress for strength of material calculations[3] or modeled as a Newtonian fluid to upgrade the code to a Navier-Stokes solver. The code includes two ablation models that allow mass addition due to solid evaporation and have been successfully employed to model ablation-fed pulsed plasma thrusters.[4] The electrons, ions and radiation field are in thermal non-equilibrium, so MACH2 solves three energy equations. These include thermal conduction with anisotropic transport[5] and three different models for radiation cooling.[6] Evolution of the magnetic field is prescribed by the induction equation that includes resistive diffusion, the Hall effect and the thermal source for magnetic fields. Various models for the plasma resistivity are available. They comprise classical anisotropic resistivity,[5] several anomalous resistivity models and contributions from electron-neutral collisions applicable to weakly ionized gases.[2] In many engineering applications the source of magnetic flux is applied currents produced from externally-applied voltage differentials. For this, the code includes a variety of circuit models such as LRC, Pulse-Forming-Networks, sine-waveforms and several others. Other additional physical models include laser-pulse energy deposition and a detonation package. The set of the MHD equations is completed by an equation of state that can be either analytic or tabular. The latter is provided by the SESAME library that includes semi-empirical models for the thermodynamic properties, transport coefficients, (including opacities) and average ionization state under local thermodynamic equilibrium. These models have been constructed and are being maintained by the T-1 and T-4 groups at Los Alamos National Laboratory.[7]

The level of sophistication and capability of the MACH2 code has been instrumental in providing invaluable insights to a variety of plasma problems. Some of these include plasma opening switches,[8] inertial-confinement fusion and alternative concepts,[9] compact toroid formation and acceleration schemes,[10] gas and solid density z-pinch implosion physics,[11] laser-target interactions,[12] high-power plasma source design,[13] magnetic nozzles[14] and a variety of plasma thrusters.[15,16] Its diverse success establishes the code as a primary numerical tool toward the understanding of the intricate physical processes and feasibility issues of the proposed propulsion concept.

PIT PHYSICAL MODELING

A substantial body of experimental data is available for the Pulsed Inductive Thruster (PIT) comprising a diverse range of propellants, energy levels and propellant mass values.[1] The power supply consists of a series of 18 capacitors in Marx-loop pairs that are charged in parallel. This results in an effective discharge voltage that is double that of the each capacitor's charge voltage which in turn provides the necessary high electric fields for breakdown. In particular, the configuration results in an effective capacitance and voltage that relate to the single capacitance and charge voltage through the total energy available:

$$E_o = \frac{1}{2}(\#\text{ of capacitors})CV_o^2 = \frac{1}{2}C_{eff}V_{eff}^2 \tag{1}$$

where V_o=1/2V_{eff}. For the polyatomic propellant experiments the effective capacitance was 9μF while the earlier efforts with monatomic propellants utilized smaller capacitors with effective capacitance of 4.5μF. The resulting oscillatory current waveform provided pulse duration of the order of 15μsec with peak currents exceeding 100kA for a range of charge voltage of 10kV<V_o<16kV and propellant mass of 1.5mg<m<10mg. Mass is introduced through a nozzle (figure 2) by a fast opening gas valve. For optimal distribution of the injected gas the mass-pulse is short enough such that it ceases as the leading edge reaches the confining lexan. The PIT's performance data exhibited approximately-constant-efficiency trends for a wide range of specific impulse values (500s<Isp<9000s) providing impulses exceeding 0.1 N-s. Monatomic propellants demonstrated efficiencies on the order of 20% while polyatomic propellants with the higher-capacitance bank dramatically improved exhibiting maximum efficiencies above 50% with ammonia.

The MACH2 simulations utilized the helium and argon data for comparisons as the SESAME tables provided a complete real equation of state that includes a degree of ionization semi-empirical model. The physical model included thermal non-equilibrium of a single-viscous fluid with classical transport. Boundary conditions modeled thermal and magnetic field insulators with no-slip. The computational grid (figure 2) extended well downstream of the thruster's exhaust region to comprehensively capture the acceleration process and assure no influence of the outlet boundary conditions that model variables at zero gradient. Grid resolution was maximized in the vicinity of the coil to assure capture of the fast-rising field's diffusion and associated gradient. In particular, the significant acceleration process occurs during the rise-time, t_r ~0.9μsec, which implies a characteristic diffusion depth of about 1.78cm for a 2eV plasma, ($\delta \sim [\eta t_r]^{1/2}$, where $\eta \sim 1000/T_e^{3/2}$ m^2/s is the electrical diffusivity with T_e in eV). The axial grid-cell dimension, Δz=1.56mm assures accurate capture of the field's gradient with more than 10 cells resolving the diffusion depth.

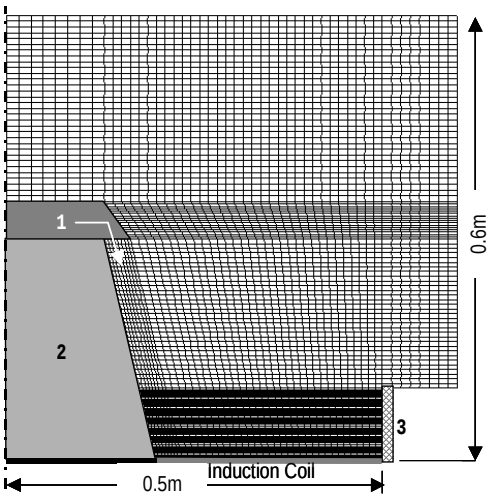

Figure 2.—Schematic of the half-plane thruster with the computational grid utilized, (to scale). 1.) Nozzle with pulsed mass-valve, 2.) Conical pylon, 3.) Confining cuff (lexan).

Table 1.—Comparison of relevant characteristics of the PIT and LRC emulated waveforms.

	PIT	MACH2-LRC
V_{eff}, E:	28kV, 1764J	28kV, 1764J
J_{max}, t_{rise}:	100kA, 0.75μs	100kA, 0.9μs
First zero, t_o:	3μs	2.7μs
J_{min}:	–40kA	–22.6kA

Initial conditions assigned uniform density in the vicinity of the coil (the confined region shown by the highest-resolution grid in figure 2) to at best resemble the evolved gas injected from the valve-and uniform room temperature. The significance of non-uniformities present due to the injection scheme is addressed later. This implies that ionization of the gas which occurs after the breakdown is calculated by the MACH2 ionization model consistently with the evolution of the rest of the pertinent variables. Emulation of the current waveform used the LRC circuit model. Specifically, a circuit model had been developed1 to calculate the PIT's current waveform with significant accuracy.[15] For the MACH2 simulation the LRC external parameters were adjusted to as-best match the important features of the aforementioned model. The comparison is shown in table 1 and the LRC current waveform used to simulate helium operation is depicted in figure 3.

It should be emphasized that the PIT circuit model included a semi-empirical statement of the plasma's inductance axial variation along with the plasma's resistance influence. The MACH2 LRC model even though it does include the influence of the latter, it does not presently include the inductance variation.

Thrust calculation was performed at the outlet boundaries as the integral of the dynamic pressure and integrated to provide the impulse. This implied that even though the effective pulse duration was about 8μs computational times needed to be in excess of 100μs so as to capture exhaust of all the propellant through the downstream boundaries. The thrust histogram for the representative case of V_o=14kV and m=3mg is shown in figure 4 along with the evolution of the impulse. The sharp rise of the thrust value at about 30μsec suggests exhaust of a compact plasma consistent with a slug-acceleration notion.

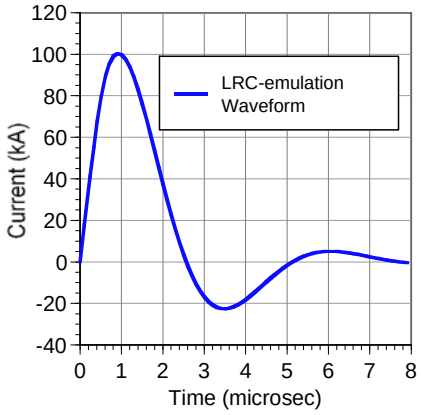

Figure 3.—Calculated Current waveform used to emulate the PIT's circuitry, V_{eff}=28kV.

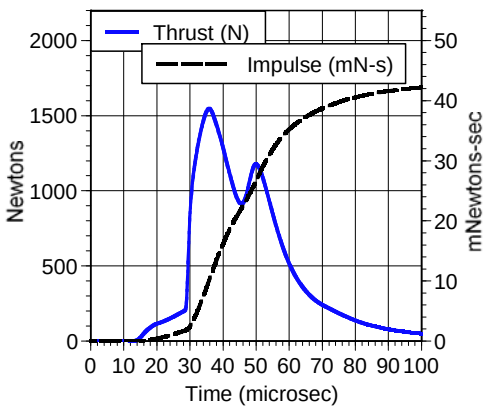

Figure 4.—Calculated thrust histogram and associated impulse evolution, V_{eff}=28kV, m=3mg.

This was confirmed by inspection of the two-dimensional density distribution as calculated by the code; they depicted a fairly sharp mass outline that included the majority of the propellant. The second peak in the evolution proposes additional acceleration of part of the remaining mass by the second peak at minimum current. The reduced gradient especially after the peak suggests a more dispersed plasma that takes longer to pass through the exhausting boundary. The width of the thrust pulse also indicates the degree of effective coupling and of course the eventual exhaust speed. In other words, a narrower histogram with higher peak thrust values would indicate better coupling and thus increased exhaust velocities for the same propellant mass and energy level. In turn, the aforementioned observations imply a substantially effective coupling of plasma and magnetic flux that allows induction of significant currents and consequently electromagnetic force. Such behavior is quite encouraging as it suggests that MACH2 captures the relevant coupling mechanisms as expected from such concept.

COMPARISONS WITH EXPERIMENT

Computations using the MACH2 code were performed for the range of available charge voltage and propellant mass. Specifically, experiments addressed a range of energy levels between 900J and 1764J with propellant mass variation from 0.75mg to 9.2mg. For each pair, data for the impulse were provided which in turn produced the range of specific impulse and efficiency values. MACH2 was invoked to compute all the different arrangements for a full range comparison of Impulse versus specific energy illustrated in figures 5 through 8. The computed impulse correlates very well with the experimental values. MACH2 computed impulse values for the 900J case exhibit an overestimation of about 10% when compared to the single experimental point. This discrepancy is partially attributed to an experimentally observed critical-mass value below which incomplete breakdown was observed along with the consequent reduction in impulse. Even though the code can not address breakdown physics, this implicit incomplete coupling of plasma and magnetic flux is partially reflected by the computations as indeed efficiency is decreasing with decreasing propellant mass value. However, the magnitude of this reduction is not fully captured by the code's physical models and thus the overestimation. It is of interest to note though, that MACH2's partial capture of this critical-mass trend is indicative of additional influencing processes other than breakdown behavior.

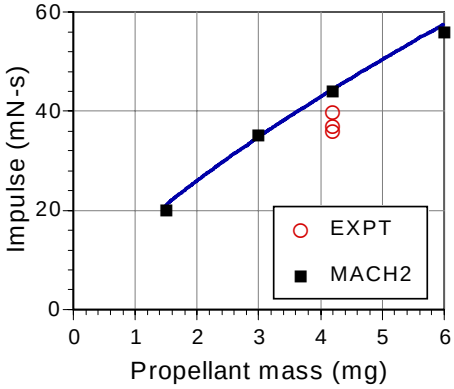

Figure 5.—MACH2 impulse comparison with experimental data for helium and 1296J.

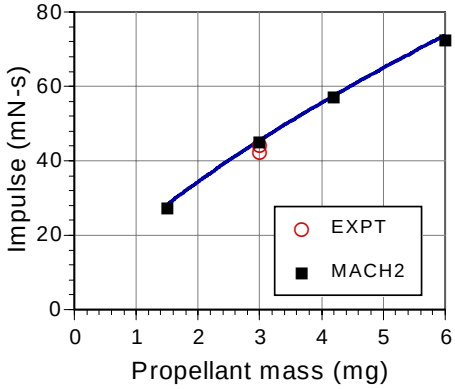

Figure 6.—MACH2 impulse comparisons with experimental data for argon and 1764J.

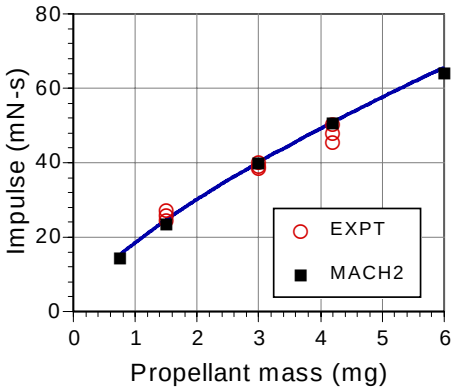

Figure 7.—MACH2 impulse comparison with experimental data for helium and 900J.

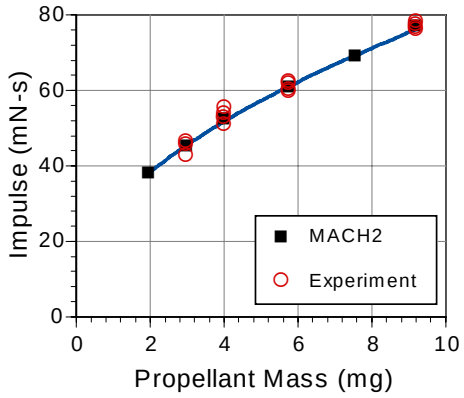

Figure 8.—MACH2 impulse comparisons with experimental data for helium and 1764J.

Even though the comparisons with experimental data are extremely encouraging certain simplifications and deficiencies of the code at its present state may be offsetting so as to result in the computed accuracy. In particular, three issues arise. Experimental data were obtained in a restricted vacuum tank of 1.2m in diameter (the thruster's diameter is 1m) while the simulations implemented a free (outlet) boundary condition for the exhausting plasma. (See figure 2, the right outermost boundary of the computational region.) The simulations assumed uniform initial conditions over the surface of the induction coil-which may tend to overestimate the calculated impulse values as uniform flux coupling is encouraged-and the lack of the LRC circuit model reaction to the plasma dynamics resulted in a current waveform that underestimates the second current peak by almost half. The latter two issues may be actually offsetting each other as any underestimation of the acceleration from the second current peak may be equalized by the aforementioned inaccuracy due to uniform initial conditions. For this the first two issues were addressed.

A new set of simulations was contrived that would emulate the vacuum tank's walls at 0.1m away from the confining lexan. This is accomplished by changing the right boundary of the computational region to a wall, no slip boundary condition. The effects and setup are clearly shown by the two-dimensional distributions of the velocity vectors (figure 9) where the latter depicts the simulation with the confining vacuum-tank wall. A comparison of the computed performance is shown in table 2 and implies insignificant influence from the restrictive vacuum tank.

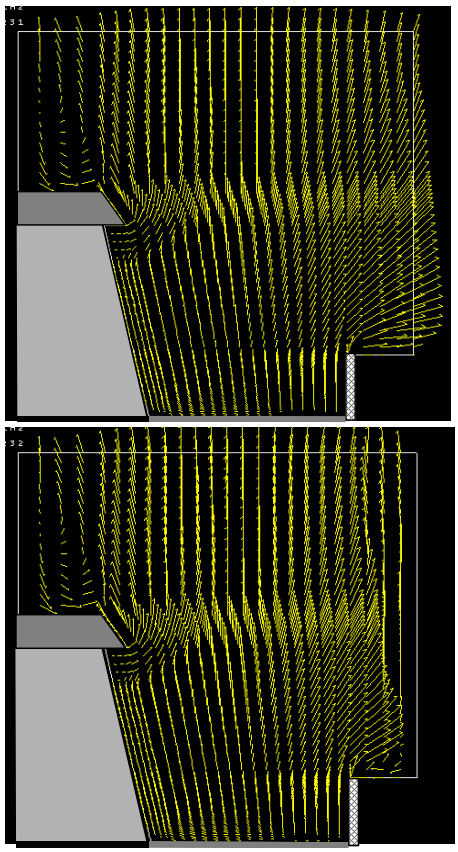

Figure 9.—Velocity vector distribution depicting the influence of the wall boundary condition. Top: Outlet, Bottom: Emulation of vacuum-tank wall at the right boundary.

Table 2.—Calculated impulse values with and without influence from the vacuum-tank wall.

E(J)/m(mg)	I (outlet)	I (tank wall)
900/4.2	44.3 mN-s	43.6 mN-s
1296/3	35.7 mN-s	35.7 mN-s
1296/1.5	26.5 mN-s	28.7 mN-s
1764/3	42.2 mN-s	43.1 mN-s

The second issue that can be addressed by the code in its present state is the mass injection scheme. The thruster utilizes a gas valve and a conical nozzle to guide the cold propellant gas toward the induction coil. The duration of the pulse in the experiments was designed such that the desired amount is injected before the leading edge of the expanding gas reaches the confining cuff. A delay before discharge followed such that all the propellant is given the opportunity to distribute itself over the induction coil. Emulation of the process by the MACH2 code introduces the mass at the conical nozzle as helium at room temperature and subsonic speeds. This choice of the mass-flow-rate value ensured injection of the total propellant in 2msec. (The particular simulation considered the 1.5mg case.) The two-dimensional mass density distributions depicted in figures 10 and 11 outline the evolution and behavior of the cold propellant as it expands toward the induction coil. At 2msec the flow rate is interrupted and the emulated

discharge is initiated which is somewhat dissimilar from the experimental setup that enforced a delay such that the mass is distributed as uniformly as possible. In other words, the MACH2 simulation will address non-uniformities from the mass-injection scheme that are much more profound than during actual operation. One of the main differences is that the MACH2 scheme prevents a significant portion of the mass to interact with the fast-rising magnetic field, (the propellant still flowing along the pylon in figure 11, 2msec).

Comparisons of the calculated impulse values between the uniformly distributed properties and this injection scheme for V_o=12kV and m=1.5mg show insignificant influence of the latter. Specifically, uniform initial conditions predict an impulse of 26.5mN-s while the more pragmatic mass-injection scheme calculates 23.9mN-s. The discrepancy is insignificant, especially considering that during the experiments the mass was given the opportunity to distribute itself as uniformly as possible before the voltage drop was applied. A plausible explanation arises from interrogation of the axial distributions of the magnetic field temperature and ionization level, but can as well be deduced by noting that only a portion of the propellant (of the order of the diffusion depth) adjacent to the coil participates in the magnetic flux coupling and current induction. This hotter, ionized fraction is subject to electromagnetic acceleration, but as it propels downstream it entrains the remainder colder propellant. This colder propellant's location is relatively inconsequential (whether it resides immediately downstream of the accelerating fraction or still expanding over the conical pylon) as it will be eventually swept by the fast moving portion.

The aforementioned deductions can be extrapolated as to the effect of the LRC model's plasma-inductance deficiency which resulted in underestimating the minimum current's magnitude by half. They imply that any additional acceleration due to the second current peak is minimal. If indeed the overestimation from assuming uniform initial conditions was originally equalized by the deficiency in calculating the acceleration due to second current peak then the latter's contribution is only of the order of (26.5-23.9)mN-s=2.6mN-s~10%. This is minimal of course partly due to the lower energy levels involved in the helium experiments and thus the relative significance of the plasma's inductance. The LRC model in MACH2 needs to be amended to include the effects of plasma dynamics before higher-energy-level modeling is performed.

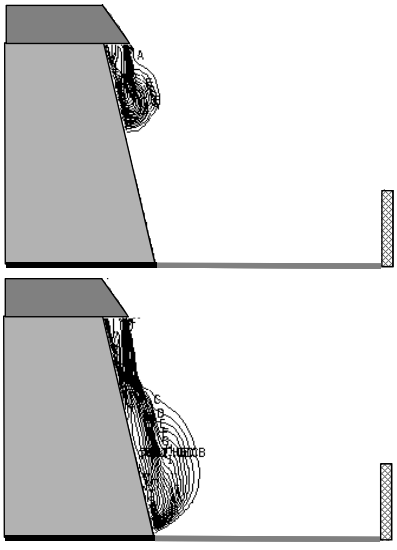

Figure 10.—Mass-density evolution as it is injected from the conical nozzle, (0.3msec and 0.8msec).

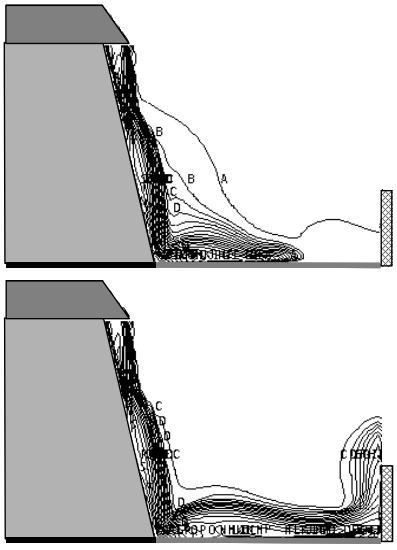

Figure 11.—Mass-density evolution as it is injected from the conical nozzle, (1.2msec and 2msec). At 2msec the emulated discharge is initiated.

THEORETICAL MODELING

In order to gain further insights into the acceleration mechanism of the Pulsed Inductive Thruster (PIT), we will construct an idealized model by assuming a purely radial magnetic field that is radially and azimuthally uniform. This can be formulated by the following expression (see figure 12), and boundary conditions:

$$B_r(z)=\frac{\mu_o J}{r_o-r_i}f(\zeta) \text{ where } \zeta=\frac{z}{z_o} \text{ and } f(0)=1;\ f(1)=0;\ \frac{d}{d\zeta}f(\zeta)\Big|_{\zeta-1}=f'(1)=0 \tag{2}$$

The function, $f(\zeta)$ is arbitrary provided it satisfies the stated boundary conditions subject to an effective current conduction zone, z_o. Application of Ampere's law produces an expression for the induced azimuthal current,

$$\nabla\times\vec{B}=\frac{1}{z_o}\frac{\partial B_r}{\partial\zeta}=\mu_o j_\theta \Rightarrow j_\theta=\frac{Jf'(\zeta)}{(r_o-r_i)z_o} \tag{3}$$

Then the purely axial electromagnetic force exerted on the plasma can be formulated:

$$F_z=\int_V j_\theta B_r dV=\int_0^1\int_0^{2\pi}\int_{r_i}^{r_o}\frac{-\mu_o J^2 f(\zeta)f'(\zeta)}{(r_o-r_i)^2}rdrd\theta d\zeta=\frac{-\pi\mu_o J^2\left(r_o^2-r_i^2\right)}{(r_o-r_i)^2}\int_0^1 f(\zeta)f'(\zeta)d\zeta \tag{4}$$

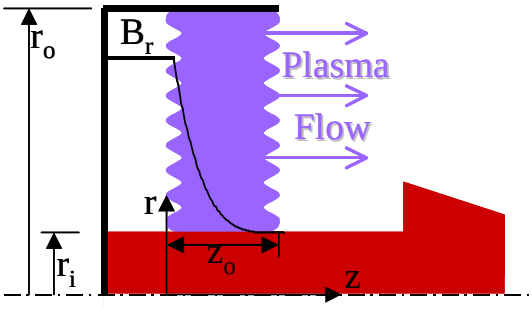

Figure 12.—Schematic of the Pulsed Inductive Thruster (PIT) utilized for the idealized model.

The value of the integral involving the axial distribution is independent of the function, $f(\zeta)$ so long it adheres to the boundary conditions; it is –1/2. Hence, the accelerating force is,

$$F_z(t)=\frac{\pi\mu_o J(t)^2(r_o+r_i)}{2(r_o-r_i)}=\frac{1}{2}L'J(t)^2 \Rightarrow L'=\frac{\pi\mu_o(r_o+r_i)}{2(r_o-r_i)} \tag{5}$$

where L' is the inductance per unit length.

If we further assume a LRC circuit configuration for the PIT we can write the governing differential equation as follows:

$$V(t) - L_e \dot{J}(t) - R_e J(t) - V_p(t) = 0; \quad V_p(t) = L_p(t)\dot{J}(t) + \left[R_p(t) + \dot{L}_p(t)\right]J(t) \tag{6}$$

where the subscript, *e* denotes the circuit's external elements and subscript, *p* denotes plasma parameters. For the idealized approach we will assume constant effective values for the plasma elements. We can identify the plasma's impedance as $Z = R_p + \dot{L}_p$, and since the plasma's inductance is $L_p = L'z_o$ we can combine to produce the idealized circuit equation:

$$V(t) - L\dot{J}(t) - [R_e + Z]J(t) = 0 \text{ where } L = L_e + L'z_o \tag{7}$$

The solution to the differential equation is the familiar LRC circuit waveform,

$$J(t) = \frac{V_o}{\omega L}\exp\left[\frac{-(R_e + Z)}{2L}t\right]\sin(\omega t); \quad \omega = \sqrt{\frac{1}{LC} - \frac{(R_e + Z)^2}{4L^2}} \tag{8}$$

that allows calculation of the following convenient integral to be utilized throughout the remainder of the model's formulation,

$$\int_0^\infty J(t)^2\,dt = \int_0^\infty \left(\frac{V_o}{\omega L}\exp\left[\frac{-(R_e + Z)}{2L}t\right]\sin(\omega t)\right)^2 dt = \frac{CV_o^2}{2(R_e + Z)} = \frac{E_o}{(R_e + Z)} \tag{9}$$

Then the total impulse generated by the accelerator is given by

$$I = \int_0^\infty F_Z(t)dt = \frac{1}{2}L'\int_0^\infty J(t)^2\,dt = \frac{L'E_o}{2(R_e + Z)} \tag{10}$$

and since $I=mU_e$ we can formulate an expression for the plasma's kinetic energy, *KE* and the energy dissipated to the circuit's external elements via resistive loss, E_R

$$KE = \frac{1}{2}mU_e^2 = \frac{(L')^2 E_o^2}{8m(R_e + Z)^2}; \quad E_R = R_e\int_0^\infty J(t)^2\,dt = \frac{R_e E_o}{(R_e + Z)} \tag{11}$$

A simple statement of conservation of energy that distinguishes these two energy modes can be written as $E_R+KE=(1-\xi)E_o$, where ξ is the fraction of the total energy deposited into the plasma via resistive heating, and dissipated due to irreversible processes. Substitution of the expressions stated above results in a second-order polynomial with respect to the quantity, R_e+Z, the positive root of which can be easily expressed as follows:

$$(1-\xi)(R_e+Z)^2 - R_e(R_e+Z) - \frac{L'^2 E_o}{8m} = 0 \Rightarrow R_e + Z = \frac{R_e + \sqrt{R_e^2 + (1-\xi)L'^2 E_o / 2m}}{2(1-\xi)} \tag{12}$$

Substitution into the impulse expression with some algebraic manipulation results

$$I = \frac{(1-\xi)L' E_o \sqrt{2m}}{R_e\sqrt{2m} + \sqrt{2mR_e^2 + (1+\xi)L'^2 E_o}}; \quad L' = \frac{\pi\mu_o(r_o + r_i)}{2(r_o - r_i)} \tag{13}$$

where the expression for the inductance per unit length is repeated for convenience. It is important to emphasize that the above manipulations imply the fraction ξ to be independent of the plasma's impedance. We also note that as the external circuit element losses are diminished (R_e–>0) or as the propellant mass, m is decreased, impulse tends toward a maximum that is a function of the square root of the propellant mass and is independent of the plasma's inductance per unit length. The impulse expression allows calculation of the specific impulse, Isp=I/mg and efficiency=I2/2mEo along with verification by comparisons to experimental data. The latter is accomplished by utilizing the experimentally deduced external resistance1, R_e=5mΩ, along with the PIT's geometry (r_o=0.5m, r_i=0.2m) for a range of propellant masses and energy levels operating with different propellants. Such comparisons are displayed in figures 13 through 15 for helium, argon and carbon dioxide propellants which show impulse versus initial energy normalized over propellant mass.

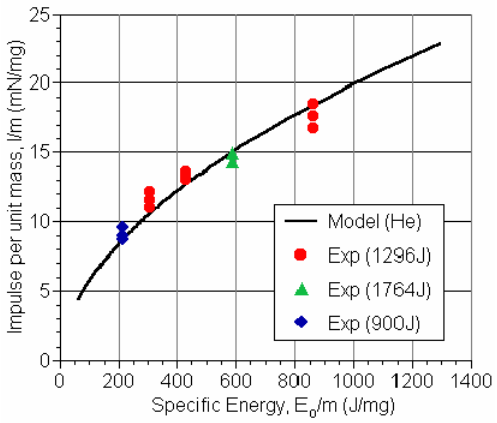

Figure 13.—Comparison of the idealized model with experimental data for helium. ξ=0.78.

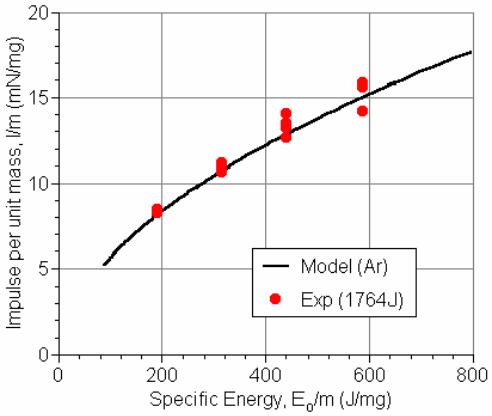

Figure 14.—Comparisons of the idealized model with experimental data for argon. ξ=0.78.

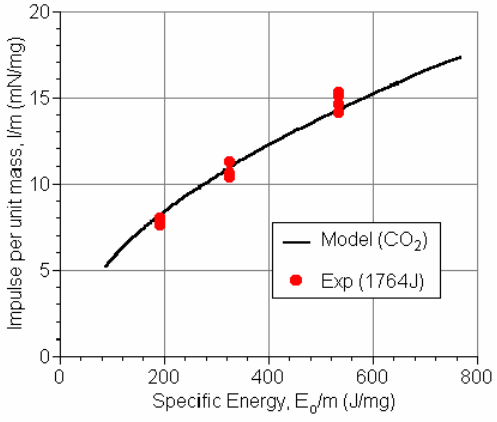

Figure 15.—Comparisons of the idealized model with experimental data for carbon dioxide. ξ=0.78.

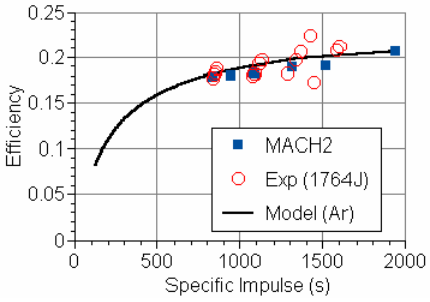

Figure 16.—Efficiency versus specific impulse for argon propellant at E_o=1764J.

The comparisons for this energy range highlight a quite unexpected trend. The fraction of the total available energy expended in heating the propellant through resistive heating (i.e., deposition of energy to heat and ionize the gas) and all other dissipating phenomena (i.e., heat transfer to the surroundings, viscous momentum losses, etc.) is independent of the propellant mass, energy level or even propellant type, it is constant at 0.78! In other words, the idealized model insinuates that for all these propellants the efficiency can not exceed 22% regardless of propellant mass value and energy level. In addition, the impulse expression indicates that the efficiency is not constant, but rather approaches a constant maximum value as propellant mass is decreased. This is due to the fact that the effect of external losses (due to R_e) diminishes as propellant mass is decreased. It is instructional to plot efficiency versus specific impulse which is displayed in figure 16 for argon propellant. We note the model's trend as it appropriately predicts that in the absence of any available kinetic energy, efficiency vanishes. Further development of the model is necessary in order to decipher the behavior of this energy dissipation factor at higher energy levels, but most importantly for ammonia and hydrazine that have produced much higher efficiency values than 0.22.

CONCLUSIONS

The magnetohydrodynamics code, MACH2 was employed to model the performance of the Pulsed Inductive Thruster (PIT) operated with helium and argon propellants within a range of 900J-1764J and propellant mass range of 0.75mg to 9.2mg. Comparisons between predicted and experimentally measured impulse values demonstrated excellent agreement. The effects of a restrictive vacuum tank used to obtain the experimental data were examined by simulating a wall, no-slip boundary condition at the location of the vacuum tank. Performance was insignificantly affected. Effects of the mass injection-scheme were also investigated for one energy and mass case to also show that performance was minimally affected by the non-uniform distribution of the injected propellant over the induction coil. An idealized model produced an expression for the impulse based on a fraction of energy expended to the internal plasma energy modes and dissipation effects. Comparisons with experimental data for this energy range (E_o<2000J) imply that this energy fraction is invariable regardless of propellant type (for three different propellants; He, Ar and CO_2), propellant mass and energy level.

REFERENCES

1. Dailey, L.C. and Lovberg, R.H., "The PIT MkV Pulsed Inductive Thruster," NASA Contractor Report 191155, July 1993.
2. Frese, M.H., "MACH2: A Two-Dimensional Magnetohydrodynamics Simulation Code for Complex Experimental Configurations," AMRC-R-874, September 1986. Also see Peterkin, R.E. and Frese, M.H., "MACH: A Reference Manual—First Edition," Air Force Research Laboratory, Kirtland AFB, Albuquerque, NM, September 1998.
3. Peterkin, R.E., Jr., and Frese, M.H., "A Material Strength Capability for MACH2," MRC/ABQ-R-1191, October 1989.
4. Turchi, P.J. Mikellides, I.G. Mikellides, P.G. and H. Kamhawi, "Pulsed Plasma Thrusters for Microsatellite Propulsion: Techniques for Optimization," Micro-Propulsion for Small Spacecraft, *Progress in Astronautics and Aeronautics*, Hardcover ISBN: 1-56347-448-4, Copyright 2000.
5. Braginskii, S.I., "Transport Processes in a Plasma," in *Review of Plasma Physics*, M.A. Leontovich, ed. Consultants Bureau, New York, 1965.
6. Douglas, M.R., "Radiation Production from Stagnating Compact Toroids Employing a Nonequilibrium Radiation Diffusion Model," Ph.D. Dissertation, U. of New Mexico, 1994.
7. Holian, K.S., ed., "T-4 Handbook of Material Properties Data Base. Vol. Ic: EOS," LA-1160-MS, Los Alamos National Laboratory, Los Alamos, NM, November, 1984.

8. Buff, J. et al., "Enhancement of the Radiation Yield in Plasma Flow Switch Experiments," MRC/ABQ-R-1171, Mission Research Corporation, Albuquerque, NM, 1988. Also see: *IEEE Transactions on Plasma Science*, 15, 6, pp. 766-771, 1987.
9. Peterkin, R.E., Jr., et al., "Simulations of Staged Solid Shell Implosions to Produce Fusion," AIAA Pre-print 95-2899, 31st AIAA Joint Propulsion Conference and Exhibit, San Diego, CA, 1995.
10. Degnan, J.H., Peterkin, R.E., Jr. et al., "Compact Toroid Formation, Compression, and Acceleration," *Physics of Fluids*, B5 (8), 2938, 1993.
11. Degnan, J.H., et al., "Electromagnetic Implosion of Spherical Liner," *Phys. Rev. Lett.*, 74 (1), 98, 1995.
12. Stamper, J.A., et al., "Aneurysms in laser-driven last waves," *Physics of Fluids*, 31 (11), 3353, 1988.
13. Mikellides, P.G., Turchi, P.J., and Mikellides, I.G., "Design of a Fusion Propulsion System, Part 1: Gigawatt-Level Magnetoplasmadynamic Source," *Journal of Propulsion and Power*, submitted Sept. 2000. Log No. B4106. IEPC Preprint 99-013.
14. Mikellides, I.G., Mikellides, P.G., Turchi, P.J. and York, T.M. "Design of a Fusion Propulsion System, Part 2: Numerical Simulation of Magnetic-Nozzle Flows," *Journal of Propulsion and Power*, submitted Sept. 2000. Log No. B4107. AIAA Preprint 00-3367.
15. LaPointe, M.R. and Mikellides, P.G., "High Power MPD Thruster Development at the NASA Glenn Research Center," AIAA–2001–3499, 37th AIAA Joint Propulsion Conference, Salt Lake City, UT, July 9–11, 2001.
16. LaPointe, M.R., Gilland, J.G., and Mikellides, P.G., "High Power Electromagnetic Thrusters for Spacecraft Propulsion," IMECE 2002–34354, 2002 ASME International Mechanical Engineering Congress and Exposition, New Orleans, LA, November 17–22, 2002.

REPORT DOCUMENTATION PAGE

Form Approved
OMB No. 0704-0188

1. AGENCY USE ONLY (*Leave blank*)	2. REPORT DATE	3. REPORT TYPE AND DATES COVERED
	December 2003	Final Contractor Report

4. TITLE AND SUBTITLE

Pulsed Inductive Thruster (PIT): Modeling and Validation Using the MACH2 Code

5. FUNDING NUMBERS

WBS–22–755–70–07
NCC3–860

6. AUTHOR(S)

Pavlos G. Mikellides

7. PERFORMING ORGANIZATION NAME(S) AND ADDRESS(ES)

Arizona State University
Department of Mechanical and Aerospace Engineering
P.O. Box 876106
Tempe, Arizona 85287–6106

8. PERFORMING ORGANIZATION REPORT NUMBER

E–14235

9. SPONSORING/MONITORING AGENCY NAME(S) AND ADDRESS(ES)

National Aeronautics and Space Administration
Washington, DC 20546–0001

10. SPONSORING/MONITORING AGENCY REPORT NUMBER

NASA CR—2003-212714

11. SUPPLEMENTARY NOTES

Prepared for the 28th International Electric Propulsion Conference cosponsored by the Centre National d'Études Spatiales (CNES), European Office of Aerospace Research and Development of the USAF, Snecma Moteurs, and European Space Agency (ESA), Toulouse, France, March 17–21, 2003. Project Manager, Steven Schneider, Power and On-Board Propulsion Technology Division, NASA Glenn Research Center, organization code 5430, 216–977–7484.

12a. DISTRIBUTION/AVAILABILITY STATEMENT

Unclassified - Unlimited
Subject Categories: 20 and 75 Distribution: Nonstandard

Available electronically at http://gltrs.grc.nasa.gov

This publication is available from the NASA Center for AeroSpace Information, 301–621–0390.

12b. DISTRIBUTION CODE

13. ABSTRACT ***(Maximum 200 words)***

Numerical modeling of the Pulsed Inductive Thruster exercising the magnetohydrodynamics code, MACH2 aims to provide bilateral validation of the thruster's measured performance and the code's capability of capturing the pertinent physical processes. Computed impulse values for helium and argon propellants demonstrate excellent correlation to the experimental data for a range of energy levels and propellant-mass values. The effects of the vacuum tank wall and mass-injection scheme were investigated to show trivial changes in the overall performance. An idealized model for these energy levels and propellants deduces that the energy expended to the internal energy modes and plasma dissipation processes is independent of the propellant type, mass, and energy level.

14. SUBJECT TERMS

Propulsion; Electric propulsion; Electromagnetic propulsion; Plasma propulsion

15. NUMBER OF PAGES

19

16. PRICE CODE

17. SECURITY CLASSIFICATION OF REPORT	18. SECURITY CLASSIFICATION OF THIS PAGE	19. SECURITY CLASSIFICATION OF ABSTRACT	20. LIMITATION OF ABSTRACT
Unclassified	Unclassified	Unclassified	